Optical testing of the LSST combined primary/tertiary mirror

Michael T. Tuell*[a], Hubert M. Martin[a], James H. Burge[a,b], William J. Gressler[c], Chunyu Zhao[b]

a Steward Observatory – The University of Arizona
527 National Championship Drive, Tucson, Arizona 85721-0061

b College of Optical Sciences – The University of Arizona
1630 E. University Blvd, Tucson, Arizona 85721-0094

c National Optical Astronomy Observatory
950 N. Cherry Ave., Tucson, Arizona 85719-4933

ABSTRACT

The Large Synoptic Survey Telescope (LSST) utilizes a three-mirror design in which the primary (M1) and tertiary (M3) mirrors are two concentric aspheric surfaces on one monolithic substrate. The substrate material is Ohara E6 borosilicate glass, in a honeycomb sandwich configuration, currently in production at The University of Arizona's Steward Observatory Mirror Lab. In addition to the normal requirements for smooth surfaces of the appropriate prescriptions, the alignment of the two surfaces must be accurately measured and controlled in the production lab. Both the pointing and centration of the two optical axes are important parameters, in addition to the axial spacing of the two vertices. This paper describes the basic metrology systems for each surface, with particular attention to the alignment of the two surfaces. These surfaces are aspheric enough to require null correctors for each wavefront. Both M1 and M3 are concave surfaces with both non-zero conic constants and higher-order terms (6^{th} order for M1 and both 6^{th} and 8^{th} orders for M3). M1 is hyperboloidal and can utilize a standard Offner null corrector. M3 is an oblate ellipsoid, so has positive spherical aberration. We have chosen to place a phase-etched computer-generated hologram (CGH) between the mirror surface and the center-of-curvature (CoC), whereas the M1 null lens is beyond the CoC. One relatively new metrology tool is the laser tracker, which is relied upon to measure the alignment and spacings. A separate laser tracker system will be used to measure both surfaces during loose abrasive grinding and initial polishing.

Keywords: metrology, interferometry, aspheric surface, survey telescope, laser tracker, alignment, computer-generated hologram, null corrector

1. INTRODUCTION

The Large Synoptic Survey Telescope (LSST) utilizes a unique three-mirror design with a 10 square degree field-of-view to be used as a full-time survey telescope, to be located at Cerro Pachón, Chile[1]. One of the unique aspects of this design is that the primary (M1) and tertiary (M3) mirrors are parts of a single monolithic substrate, made of Ohara E6 borosilicate glass, spin-cast over a honeycomb mold. The primary mirror diameter is 8.4-m and the embedded tertiary has a diameter of 5.0-m, shown in Figure 1. The relative alignment of the two surfaces will be set during fabrication, without the option of on-mountain adjustments. This means that the surfaces must have the correct prescriptions, be smooth, and the relative alignments to be within tolerance prior to shipment to Chile. This paper discusses the prescription, optical test methods for each surface, and the metrology to verify alignment.

*mtuell@email.arizona.edu 1-520-621-1022 ; fax 1-520-621-1578 mirrorlab.as.arizona.edu

Modern Technologies in Space- and Ground-based Telescopes and Instrumentation, edited by Eli Atad-Ettedgui, Dietrich Lemke, Proc. of SPIE Vol. 7739, 77392V · © 2010 SPIE · CCC code: 0277-786X/10/$18 · doi: 10.1117/12.857358

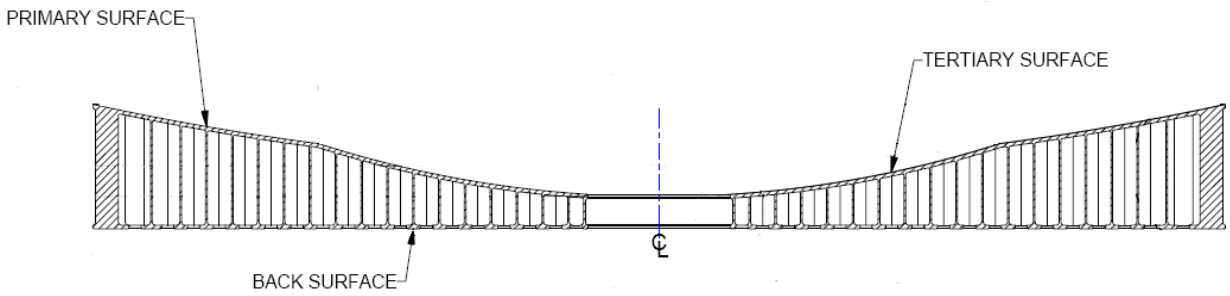

Figure 1. Cross-section view of LSST M1/M3 monolithic substrate. The outside diameter is 8417 mm and the inside diameter is 1055 mm.

The test tower at the Steward Observatory Mirror Lab is a multipurpose tower, sharing space with other mirrors. This means that LSST testing cannot interfere with other testing, and vice versa, so the two test packages must deploy from parked positions which are outside of the other light cones to the test position near the center of the tower. This is accomplished with traveling bridges which hang from structural steel in the tower. One major ramification of supporting the M3 test package is that the M3 test obscures the M1 test, if deployed simultaneously. This will be discussed further in section 5.4. The tower with LSST is shown in Figure 2.

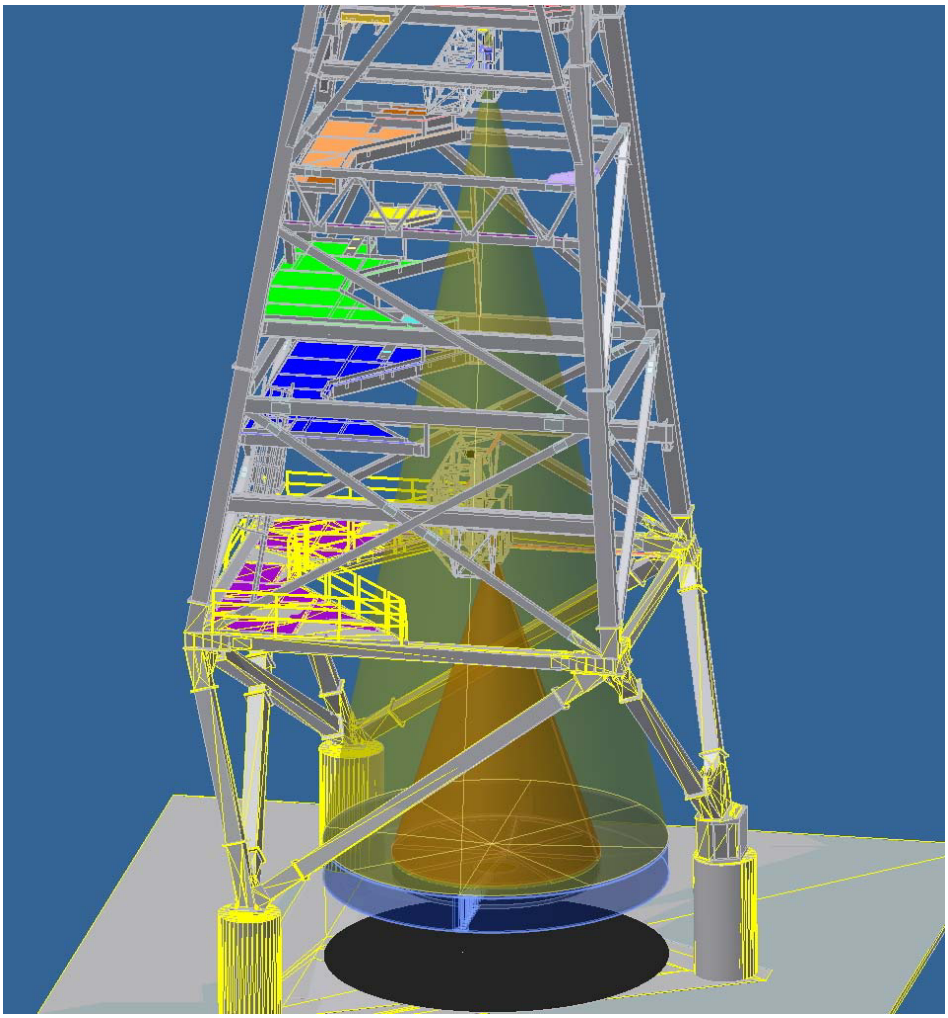

Figure 2. Test tower with LSST and both M1 and M3 bridges deployed.

2. PRESCRIPTION

2.1 Primary mirror (M1)

Table 1. M1 prescription

Parameter	Value	Tolerance	Units
Outside diameter	8417	± 1	mm
Inside diameter	NA		
Outside clear aperture diameter	8360	minimum	mm
Inside clear aperture diameter	5116	maximum	mm
Vertex radius of curvature (at 22°C)	19835.5	± 1	mm
Conic constant	-1.2150	± 0.0002	
6^{th} order term	-1.381E-24		mm^{-5}

2.2 Tertiary mirror (M3)

Table 2. M3 prescription

Parameter	Value	Tolerance	Units
Outside diameter	NA		
Inside diameter	1054.7	+2 / -0	mm
Outside clear aperture diameter	5016	minimum	mm
Inside clear aperture diameter	1100	maximum	mm
Vertex radius of curvature (at 22°C)	8344.7	± 1	mm
Conic constant	+0.155	± 0.0001	
6^{th} order term	4.5E-22		mm^{-5}
8^{th} order term	8.15E-30		mm^{-7}

2.3 Mechanical and alignment

Table 3. Mechanical alignment prescription

Parameter	Value	Tolerance	Units
Substrate thickness at R = 4208.5 mm	919	± 2	mm
Substrate wedge	0	< 30	arc seconds
M1 mean facesheet thickness	28	± 1	mm
M3 mean facesheet thickness	28	± 1	mm
M1 vertex to substrate mechanical center	0	< 1	mm
M3 vertex height below M1 vertex	233.8	± 2	mm
M1-M3 relative tilt	0	< 100	microns TIR
M1-M3 axis displacement	0	< 1	mm

The joint radial location of the two surfaces is nominally at 2533 mm radius, but there is no tolerance on this parameter. This location is determined by the two as-built surface prescriptions and the vertical offset between surfaces, so as long as the prescriptions and clear aperture specifications are met (between 5016 mm / 2 and 5116 mm / 2 (2508 mm to 2558 mm)) it is irrelevant where the actual transition point is.

3. FABRICATION SUMMARY

Interested readers should refer to previously published papers[2-5] for more information on fabrication techniques used at the Steward Observatory Mirror Lab.

The Steward Observatory Mirror Lab makes honeycomb sandwich mirror blanks from Ohara E6 borosilicate glass. The first step is to create a mold from ceramic refractory material on top of which 3 to 10 pound chunks of glass are laid. Heating the furnace to 1165°C allows the glass to melt into a honey-like consistency and flow down into the mold. Very slow controlled cooling (3-4 months) allows proper annealing of the glass. Once cool, the blank is lifted off the hearth and the mold is washed out with high-pressure water. The flat rear surface is then processed with fixed-abrasive diamond generating, loose-abrasive grinding with a lap and finally polishing with a lap. The finished rear surface has load-spreaders and hard-points glued on. The mirror is then flipped over and put into a polishing cell. Front surface processing then begins with the same sequence of abrasives used on the rear surface, except the lap is not flat – in fact it is an actively bent stressed lap which matches the shape of the surface at all points. A laser tracker or IR interferometer is used to guide loose-abrasive grinding and initial polishing. Once polished out, the surface is measured with visible light interferometry as the ultimate test of surface accuracy.

As of this writing (the end of May, 2010), the mirror has been cast and has rear-surface processing completed. The mirror is now in the polishing cell and coarse diamond generating is complete. The fine diamond generating is complete for M3 and has just begun for M1. After M1 is complete, edging and beveling to the finished diameters will be done and then loose-abrasive grinding will commence. Figure 2 shows recent photos of the mirror blank on the generator, with a black circle drawn to the approximate transition point between M1 and M3.

Figure 3. Recent photographs of the generating process, top view and side view. (Courtesy of Jeff Kingsley)

4. OPTICAL TEST SYSTEMS

4.1 Aspheric departure

The departures from the best-fit spheres are 610 µm for M1 and 389 µm for M3, as seen in Figure 4. M1 has a negative conic constant, so has negative spherical aberration, while M3 has a positive conic constant, so has positive spherical aberration. Neglecting higher-order deformation terms, M1 is hyperboloidal, while M3 is an oblate ellipsoid. These require very different testing configurations, as we will see in the next sections.

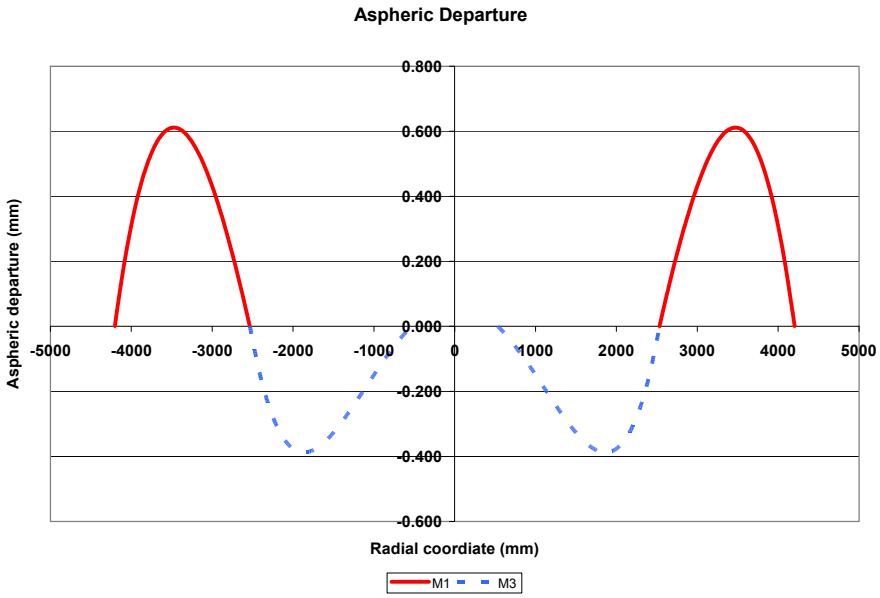

Figure 4. Aspheric departure for both surfaces. The radii are very different, as well as having a vertical offset between vertices, so it does not form a continuous surface as depicted (see Figure 1 for the actual curves).

4.2 Primary mirror

Typical primary mirrors for telescopes are paraboloidal, or nearly so, whereas LSST M1 has an even flatter profile than a paraboloid. However, the primary mirror focal ratio (f/1.18) is nearly the same (f/1.14) as for the Large Binocular Telescope (LBT) primary mirrors[2]. Since the null corrector for LBT still exists, it was determined that a simple re-spacing of the elements would create an acceptable wavefront to test LSST M1. This null lens is a two element Offner null corrector with a fast relay lens (which creates the vast majority of the spherical aberration required) and a field lens which goes just outside of the center of curvature of M1. Figure 5 shows the layout of the test system. Notice how little of the relay lens is being used due to the 5-m "hole" in the middle of M1.

A small concave spherical mirror can be temporarily placed below the focal point of the interferometer, such that the center of curvature of the small sphere is at the focal point within 20 microns in X, Y, and Z. The majority of this error is in the uncertainty of placement of this mirror, rather than the optical alignment to it. This allows accurate placement of the interferometer in XYZ to align the beam to the null corrector.

4.3 Tertiary mirror

A simple refractive null corrector for an oblate ellipsoid is difficult without an aspheric surface, so a phase-etched computer-generated hologram (CGH), used in transmission, was selected instead. Outside of the main transmission pattern, there is an annular region of chrome-on-glass binary rings, used in reflection, which allows the interferometer to be aligned in XYZ to the hologram. This system is also shown in Figure 5. The focal ratio of M3 is a fairly fast f/0.82.

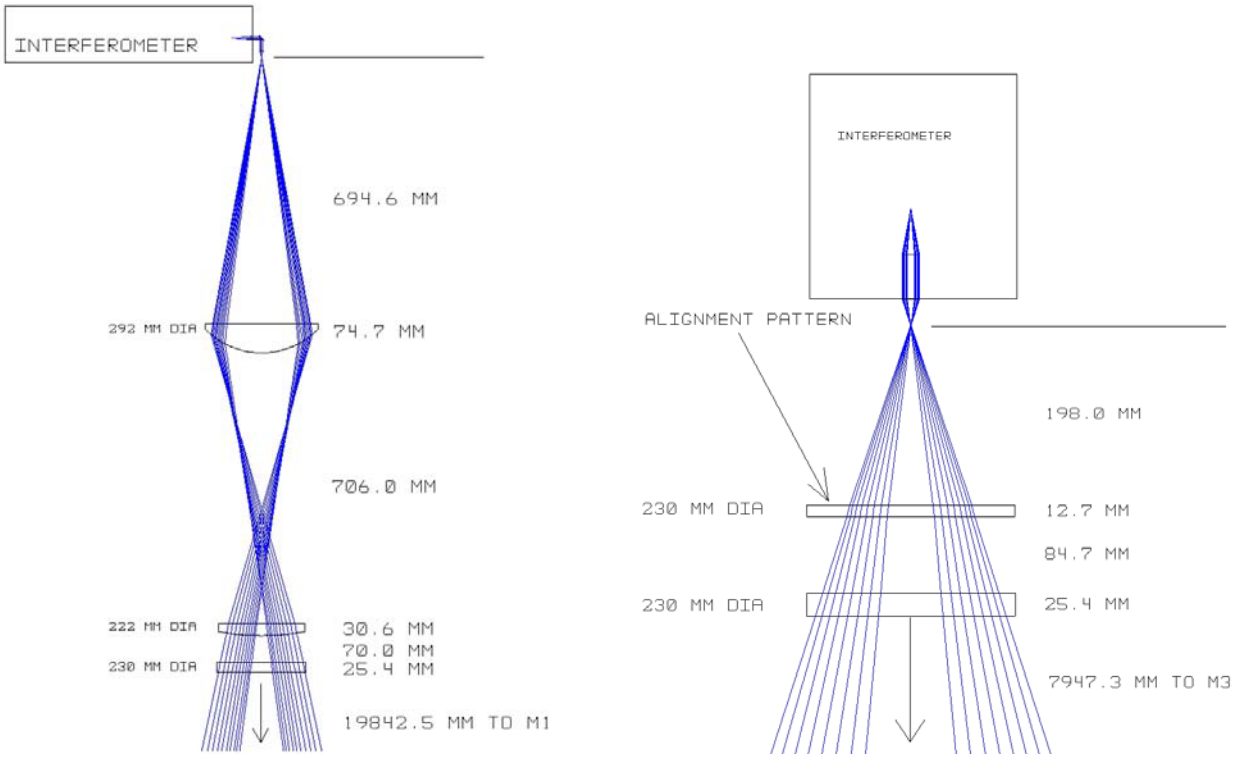

Figure 5. M1 Offner null corrector on the left and the M3 phase-etched CGH null corrector on the right. The bottom element of each system is a removable certifier CGH. Both interferometers are Twyman-Green instantaneous phase-shifting devices (PhaseCam® 4000 series) from 4D Technology, Inc. (Not to the same scale).

5. OPTICAL TOLERANCES

5.1 Structure functions

Ground-based telescopes are specified so as not to degrade the wavefront delivered by the atmosphere. In seeing-limited observations, the telescope optics will contribute little to the image blur. In diffraction-limited observations with adaptive optics, the telescope optics will add little to the stroke of the deformable mirror. The wavefront delivered by the atmosphere has a spectrum of errors described by a structure function[6], which gives the mean square difference in wavefront between points in the pupil as a function of their separation. The same form of structure function is used to specify the wavefront accuracy of the LSST mirrors. The magnitude of allowed error is defined by the Fried parameter, r_0. In addition, an allowance is made for small-scale structure that scatters a small fraction of the light outside the seeing-limited disk. Finally, because active guiding removes the global wavefront tilt, the structure function specification is tightened on large scales to remove the contribution of tilt. The form of the structure function that accounts for all three effects is shown in Eq. 1.

$$\delta^2(x) = \left(2\sigma^2 + \left(\frac{\lambda}{2\pi}\right)^2 6.88 \left(\frac{x}{r_0}\right)^{5/3} \left(1 - 0.975\left(\frac{x}{D}\right)^{1/3}\right)\right) \quad (1)$$

Where $\delta^2(x)$ is the mean-square wavefront difference between points on the mirror separated by x, σ is the rms wavefront error in small-scale structure, r_0 is the Fried parameter, and D is the diameter of the mirror for tilt compensation. Both σ

and r_0 are given in Table 4 for a wavelength of 500 nm. To convert from a scattering loss to a wavefront error we can use Eq. 2.

$$L = 1 - e^{-\left(\frac{2\pi}{\lambda}\sigma\right)^2} \quad \text{or} \quad \sigma = \left(\frac{\lambda}{2\pi}\right)\sqrt{-\ln(1-L)} \tag{2}$$

For example, 2% loss (L = 0.02) at 500 nm represents σ = 11.3 nm.

Table 4. Structure function and microroughness specifications for both M1 and M3.

Parameter	Value	Tolerance	Units
Fried parameter at zenith (at 500 nm) for M1	92		cm
Fried parameter at zenith (at 500 nm) for M3	151		cm
Scattering at λ = 500 nm	2 % (goal 1.5 %)	maximum	%
Microroughness on scales << 1 cm	20 (goal 10)	maximum	Å rms

Typically, structure functions are plotted as the square-root of Eq. 1, which is then the RMS wavefront difference between points. The difference between the specification and goal is only meaningful at scales below 200 mm, in this case. At the smallest separations (one pixel), there is a difference of about 2 nm between the specification and goal.

Since even calibrated measurements have some uncertainty, we need to define a measurement specification, which is slightly tighter than the mirror specs, to account for this uncertainty. The losses add linearly, so if we make the assumption that 0.4% loss is attributable to the test system, then the target for the measurement is 1.6% loss, which adds to the 2% specification for the mirror. Computing the Fried parameters is less straightforward, adding neither linearly or quadratically. Eq. 1 shows that the Fried parameter is scaled to the minus 5/3 power, so we add the two Fried parameters to the -5/3 power then take the sum to the -3/5 power. If we assign the test system a Fried parameter of 240 cm, then the measured figure must meet a Fried parameter of 105 cm. Appropriately adding these give the mirror spec of 92 cm. Similarly, for M3, if the test system contributes 0.4% loss and has a Fried parameter of 400 cm, then the measured figure must meet 1.6% loss and a Fried parameter of 172 cm. The test system and measured figure graphs, shown in Figure 6, do add quadratically to the mirror specifications, since they are RMS wavefront differences.

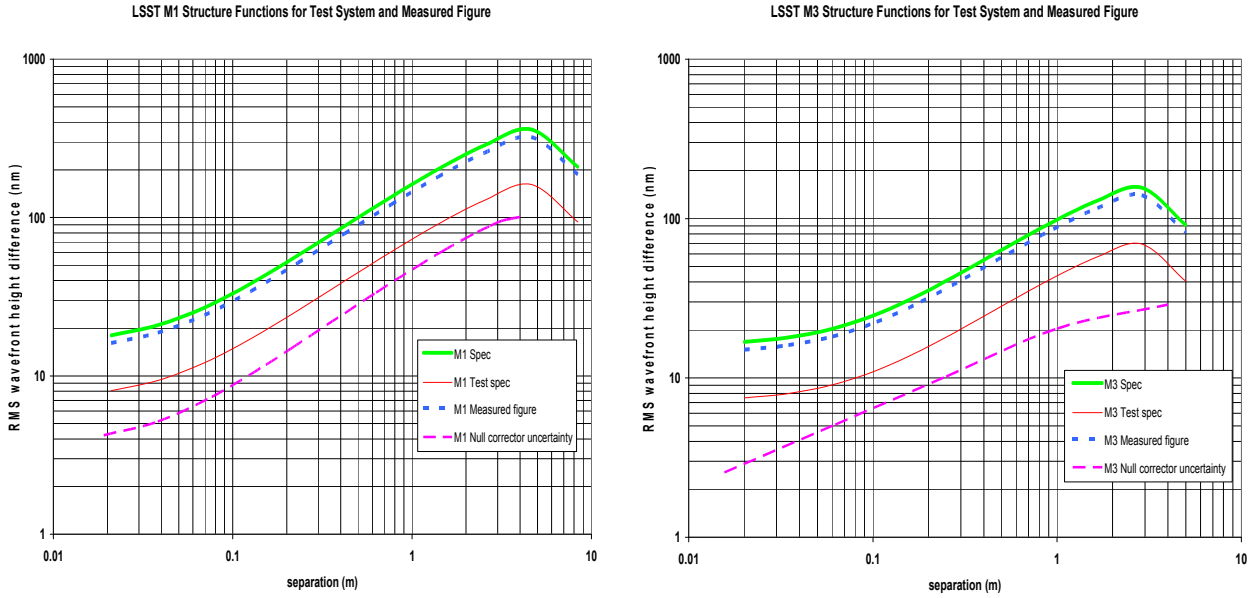

Figure 6. Test system, measured figure, and mirror specification structure functions, as well as the uncertainty in null corrector wavefronts for M1 (left) and M3 (right).

We now have specifications for the sum of all test system errors. This test system spec is shown in Figure 6 as the solid thin line, and the expected uncertainty in the null correctors are shown as the thin dashed line (the lowest curves). Note that these structure functions ignore errors in radius and conic constant, since those are specified independently.

The radii of curvature, conic constants and axis decenters are independently specified, so if they are in tolerance, power, third-order spherical aberration, and third-order coma can be removed from the data. As discussed in section 5.4, bending modes of reasonable amplitude may also be removed. The higher-order deformation terms have no tolerance, so any errors in them are considered to be figure error which is reflected in the structure function.

5.2 Radius of curvature

Two basic methods will be used to measure the vertex radii – laser tracker scans of the surfaces show deviations in radius, as well as other errors, and a laser tracker measuring reference points near the edge of the surface in comparison with where the (aligned) CGH is located. Since the radii have explicit tolerances, power can be removed from all surface maps providing the radii are within tolerance.

5.3 Conic constant

Since the conic constants have explicit tolerances, third-order spherical aberration can be removed from the data prior to structure function analysis as long as it is within spec. The null correctors have uncertainties within tolerance inherently, but each system also has a certifier CGH[7] which independently has sufficient accuracy[8] to show compliance with the conic constant tolerances.

The method used to compute the conic constant uncertainty is to perturb a parameter, such as the index of refraction of a lens, by the uncertainty in each parameter (in this case, 95% confidence interval is used) and re-optimize the wavefront using a focal distance to compensate power and the conic constant of the mirror under test as the spherical aberration compensator. Then the difference between nominal and re-optimized conic constant is recorded for each perturbation. These differences are then summed in quadrature to find the final uncertainty.

The largest contributors to wavefront uncertainties in the Offner system are the two indices of refraction, the uncertainty in airspace between lenses and the radii of the field lens surfaces. The largest contributors to the M1 certifier CGH uncertainty are the laser frequency, air pressure and temperature (in use) and the substrate figure. For the M3 phase-etched CGH, the largest contributors are the distance to the interferometer focus and the self-weight deflection of the substrate. For the M3 certifier CGH, the largest contributors are the self-weight deflection and figure errors of the substrate.

Table 5. Uncertainty in conic constant for M1 (tolerance ± 200 * 10^{-6}) and M3 (tolerance ± 100 * 10^{-6})

Test system	**Uncertainty in conic constant (*10^{-6})**
M1 null corrector	170
M1 certifier CGH	21
M3 null corrector	35
M3 certifier CGH	5

5.4 Bending modes

All large telescopes have active primary mirrors, which allow pointing and bending to accommodate mechanical and thermal changes in surface figure. A simple flat circular disc has well known analytically derived bending modes, where

a honeycomb sandwich mirror blank requires a finite element analysis to compute the surface shapes and required forces to bend the mirror with actuators at the appropriate locations. The sum of all desired bending modes must of course be within the force budget, but within this range, it is allowable to mathematically subtract appropriate combinations of bending modes to show the theoretical optimum residual figure. This means that it is not required to polish out, for example, 100 nm of astigmatism – it will be simply bent out during use in the telescope.

LSST, being two mirrors on one common substrate, presents a unique challenge, since all bending modes affect both mirror surfaces simultaneously. Compliance to both sets of specifications will be demonstrated with simultaneous measurements, or the functional equivalent of simultaneous measurements. The primary difficulty in a true simultaneous measurement is the obscuration of the M1 test by the M3 bridge. This obscuration is shown in Figure 7. As you can see, there are six distinct "islands" of data in M1 which must be leveled to give a valid representation of the surface. The size of the obscuration was minimized without compromising the desired strength and stiffness of the bridge. There are two layers to the bridge, but they are not directly above each other – they are offset such that from the perspective of the M1 test, only a single set of beams is visible. What obscuration occurs over M3 is irrelevant to the M1 test. The bridge is "bent" to accommodate a caged ladder which is the only access from level 2 of the test tower down to level 1, where the M3 bridge stows outside of the other light cones. Furthermore, for simultaneous testing, the M3 interferometer will have a ventilation system to dump heat outside of the tower to reduce air turbulence as seen from the M1 test.

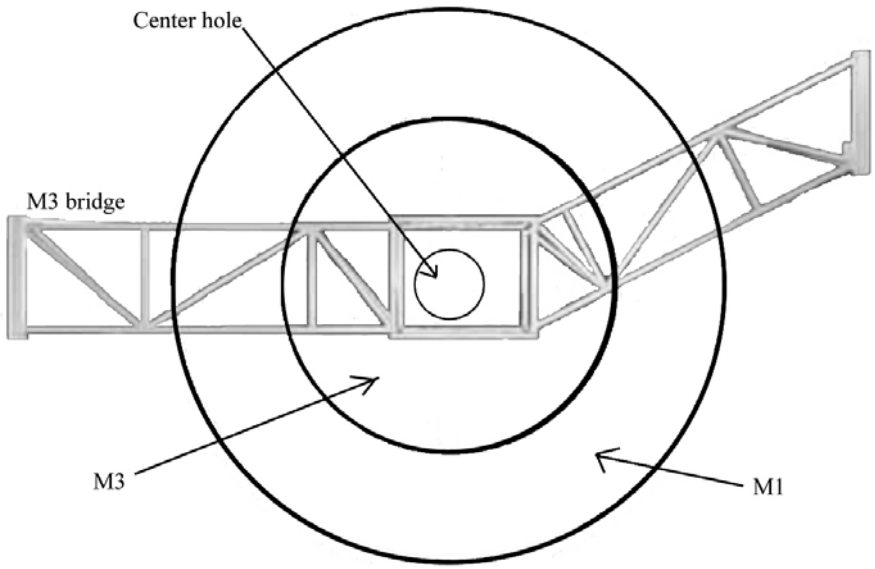

Figure 7. Perspective view of M1/M3 from the M1 test position showing the obscuration of M1 by the M3 bridge.

6. MECHANICAL AND ALIGNMENT TOLERANCES

6.1 Diameters

The outside diameter of M1 is measured with a π -tape, which accurately measures the circumference and divides by π. The inside diameter of M3 is measured with an inside micrometer. Both are accurate to well under a millimeter.

6.2 Thickness and wedge

The blank thickness is measured at a minimum of three points around the mirror with large outside calipers. The movable jaw has a ½ inch ball glued to it at a known distance from the known OD of the mirror, which allows computation of the thickness at the desired radial position. Fitting a plane to the measurements gives us a wedge angle between the backsheet and the facesheet.

6.3 Facesheet thickness

The facesheet thickness is measured with an ultrasonic probe at over 100 locations spanning the mirror. While individual data points may have uncertainties of several thousands of an inch due to the rough cut surface, these effects are reduced by averaging many points to obtain the mean facesheet thickness.

6.4 Vertex vertical displacement

The vertical displacement between the two vertices is measured with a laser tracker scanning the surfaces and fitting the data to the nominal prescriptions. Measuring both mirrors in the same coordinate system allows us to calculate the vertical displacement to within 0.25 mm, with a tolerance of ± 2 mm. Knowledge of the prescriptions allows caliper measurements at the ID of M3 and the OD of M1 to give and independent measurement of the vertex vertical displacement, as well.

6.5 M1 axis decenter

Decenter of the optical axis with respect to the mechanical axis of the mirror blank must be kept within 1 mm. This will be measured with two independent tests for verification. The first method has been used with many of the large mirrors produced at the Steward Observatory Mirror Lab. It involves defining the mechanical center, aligning the test optics to the mirror surface, rotating the mirror 180° about the mechanical center and measuring the coma produced by this rotation. Knowledge of the prescription allows us to compute the misalignment of the two axes.

The second method involves a projected spot, from a diffraction pattern on the certifier CGH, which falls on a CCD near the mirror vertex with a known relationship to the mechanical axis. As shown in Tables 7 and 8, the largest contributors to uncertainty are the alignment of the certifier CGH for M1 to the null corrector. The projected spots are very slow beams – M1 is on the order of f/520 and M3 (since it is closer) is f/210.

Table 6. Uncertainty in optical axis position of M1 for rotation test.

Source of error	**Uncertainty in each axis**	**Error in position of optical axis**
Measurement of coma at 0°	60 nm rms wavefront	0.06 mm
Measurement of coma at 180°	60 nm rms wavefront	0.06 mm
Measurement of mechanical axis at 0°	0.2 mm	0.14 mm
Measurement of mechanical axis at 180°	0.2 mm	0.14 mm
RSS		**0.22 mm**

Table 7. Uncertainty in optical axis position of M1 for projected spot test.

Source of error	**Error in position of optical axis**
Mirror alignment to null corrector, 60 nm rms wavefront coma	0.14 mm
CGH alignment to null corrector of 1 fringe of tilt (requires 0.7 μm centration)	0.21 mm
CGH mechanical decenter stability w.r.t. null corrector of 0.8 μm	0.24 mm
Calibration or control of CGH wedge to 2 arc-seconds	0.1 mm
Null corrector tilt stability 1 arc-seconds	0.1 mm
Measurement of image position with camera	0.1 mm
Transfer of image coordinates to M1 datum	0.1 mm
RSS	**0.4 mm**

6.6 M3 axis tilt and decenter

In addition to the 1 mm tolerance on M1 optical axis to M3 optical axis decenter, there is a specification for runout at the edge of M3 compared to M1 of 100 microns total indicator runout (TIR). This will be measured with LVDTs as the mirror rotates and can also be seen in laser tracker scans of the surfaces. It is difficult to control the tilt to better than about 25 microns, but the measurement should be accurate to about 10 microns.

The rotation test for M3 has slightly more uncertainty in the coma measurement (0.07 mm for each rotation, as compared to 0.06 mm for M1 – see Table 6), which results in essentially the same net uncertainty of 0.22 mm.

Since the null corrector for M3 is a hologram, we can put the projected spot pattern directly on the null corrector, as opposed to the certifier CGH for M1. Therefore, measurement of the axis with the projected spot test is more accurate for M3 than M1 because there is no need to align the certifier hologram to the null corrector.

Table 8. Uncertainty in optical axis position of M3 for projected spot test.

Source of error	**Error in position of optical axis**
M3 alignment to null corrector, 60 nm rms wavefront coma	0.1 mm
Alignment of interferometer reference surface to 1 fringe (0.2 fringes across 40 mm)	0.025 mm
Measurement of image position with camera	0.1 mm
Transfer of image coordinates to mechanical axis datum	0.1 mm
RSS	**0.18 mm**

7. CONCLUSION

We have shown the methods for testing the LSST M1/M3 combined mirror, with regard to each mirror prescription and the interaction between mirror surfaces. Analysis of uncertainties in each test have been shown to meet the required accuracy for each test, which means that the required accuracy for the M1/M3 system can be achieved. This has been shown for the radii of curvature, conic constants, and residual figure errors (structure functions) as well as the mechanical and alignment specifications of diameters, wedges, decenters, and the relative vertex spacing.

ACKNOWLEDGEMENTS

LSST is a public-private partnership. Design and development activity is supported by in part the National Science Foundation under Scientific Program Order No. 9 (AST-0551161) and Scientific Program Order No. 1 (AST-0244680) through Cooperative Agreement AST-0132798. Additional funding comes from private donations, grants to universities, and other LSST Corporation Institutional Members. The project is overseen by the LSST Corporation, a non-profit 501(c)3 corporation formed in 2003, with headquarters in Tucson, AZ.

REFERENCES

[1] Sweeney, D. W., "Overview of the Large Synoptic Survey Telescope project", in *Ground-based and Airborne Telescopes*, ed. L. M. Stepp, Proc. SPIE 6267, 626706 (2006).

[2] Martin, H. M., Allen, R. G., Burge, J. H., Dettmann, L. R., Ketelsen, D. A., Miller, S. M. and Sasian, J. M., "Fabrication of mirrors for the Magellan Telescopes and the Large Binocular Telescope", in *Large Ground-based Telescopes*, ed. J. M. Oschmann and L. M. Stepp, Proc. SPIE 4837, p. 609-618 (2003).

[3] Martin, H. M., Allen, R. G., Cuerden, B., Hill, J. M., Ketelsen, D. A., Miller, S. M., Sasian, J. M., Tuell, M. T. and Warner, S., "Manufacture of the second 8.4 m primary mirror for the Large Binocular Telescope", in *Optomechanical Technologies for Astronomy*, ed. E. Atad-Ettedgui, J. Antebi and D. Lemke, Proc. SPIE 6273, 62730C (2006).

[4] Martin, H. M., Burge, J. H., Cuerden, B., Davison, W. B., Kingsley, J. S., Lutz, R. D., Miller, S. M. and Tuell, M. "Manufacture of a combined primary and tertiary mirror for the Large Synoptic Survey Telescope", in *Advanced Optical and Mechanical Technologies in Telescopes and Instrumentation*, ed. E. Atad-Ettedgui and D. Lemke, Proc. SPIE 7018, 70180G (2008).

[5] West, S. C., Martin, H. M., Nagel, R. H., Young, R .S., Davison, W .B., Trebisky, T. J., DeRigne, S. T. and Hille, B. B., "Practical design and performance of the stressed lap polishing tool", *Applied Optics*, 33, p. 8094-8100 (1994).

[6] Martin, H. M., Allen, R. G., Angel, J. R. P., Burge, J. H., Davison, W. B., DeRigne, S. T., Dettmann, L. R., Ketelsen, D. A., Kittrell, W. C., Miller, S. M., Strittmatter, P. A. and West, S. C., "Fabrication and measured quality of the MMT primary mirror", in *Advanced Technology Optical/IR Telescopes VI*, ed. L. M. Stepp, Proc. SPIE 3352, p. 194-204 (1998).

[7] Burge, J. H., "Certification of null correctors for primary mirrors", in *Advanced Optical Manufacturing and Testing IV*, J. Doherty, Editor, Proc. SPIE 1994, p. 248-259 (1993).

[8] Zhou, P. and Burge, J. H., "Optimal design of computer-generated holograms to minimize sensitivity to fabrication errors", *Opt. Express,* 15, p. 15410-15417 (2007).